Performance of droop-controlled microgrids with heterogeneous inverter ratings

H. Giray Oral and Dennice F. Gayme

***Abstract*— This paper characterizes synchronization performance and total transient power losses in droop-controlled microgrids with heterogeneously rated inverters. We consider frequency and voltage dynamics for a Kron-reduced network model with highly inductive lines in the presence of impulse disturbances. We quantify the total transient frequency and voltage deviations from synchrony and the associated total transient resistive losses through the $\mathcal{L}_2$ norm of the system output. We derive closed-form expressions for this norm that depend on the heterogeneous droop gains and properties of the network. Our results indicate the importance of inertia in mitigating transient frequency deviations. We also show that if disturbances are uniform, the transient resistive losses are given by a monotonically decreasing function of the active power droop gains regardless of the network topology. Numerical examples further analyze these losses, revealing that they can be amplified by high droop gain heterogeneity. This relationship indicates that non-uniform power sharing requirements can limit performance.**

I. Introduction

Stable operation of a microgrid requires frequency and voltage synchronization. Power sharing, which is the distribution of power demand between the generation units, is also an important measure of the system efficiency [1]. Stability and power sharing in inverter based microgrids are typically achieved through droop control; a decentralized proportional control action on the frequency and voltage [2]. Conditions ensuring frequency synchronization and active power sharing have been obtained for microgrids modeled through their frequency dynamics, assuming constant voltages [3]. Models also including voltage dynamics yield conditions for both frequency and voltage synchronization [4], [5] as well as reactive power sharing [6]. Recent work uses a higher order model accounting for line current dynamics to obtain more comprehensive stability conditions [7].

Other measures of system performance and efficiency include robustness and the transient resistive power losses sustained in maintaining synchrony when the system is subjected to distributed disturbances. These transient resistive losses have been investigated using the linearized swing dynamics of a Kron-reduced transmission network [8], a structure preserving network model of a renewable energy integrated power system [9], as well as a model of droop-controlled microgrids with coupled frequency and voltage dynamics [10]. Related work uses $\mathcal{H}_2$ norm based analysis to examine the robustness in second order consensus networks [11], [12] and low-inertia power systems with constant voltage [13]. Control nodes [14] and virtual inertia placement [15] have been proposed to optimize the synchronization performance in constant voltage transmission grids. Dynamic control strategies such as distributed PI-control have been shown to reduce transient resistive losses [16]. A dynamic droop control based on lead-lag compensation has also been shown to improve noise and delay robustness [17].

Much of the literature focuses on identical nodal dynamics, which simplifies the analysis significantly while still providing insight into the robustness of droop control [10]. However, this simplified setting prevents the investigation of a number of important situations that can arise in practice. For example, power sharing constraints resulting from a load demand that is heterogeneous across the network lead to heterogeneous droop gains [3], [5]. There has been some work in transmission systems with heterogeneous inertias, which provides a step response characterization of the synchronous system frequency [18]. In a similar setting, the interaction between the network topology and this synchronous frequency is studied [19]. However, extensions to microgrids which are typically far less uniform by design have yet to be addressed.

In this work we analyze the robustness of droop-controlled microgrids with heterogeneously rated inverters modeled by both frequency and voltage dynamics. We consider two performance measures in the presence of distributed impulse disturbances. The first one quantifies the total transient frequency and voltage deviations from the synchronous state while the other quantifies the associated total transient resistive losses. Both measures are captured through the $\mathcal{L}_2$ norm of the system output. We derive closed-form solutions for these measures in terms of the heterogeneous droop gains and properties of the network for the case of highly inductive lines (i.e. decoupled frequency and voltage dynamics). We show that the transient deviations from synchrony prevail even in the hypothetical case of infinite droop gains (i.e. infinite control action), which points to the importance of inertia in further mitigating these oscillations. We also show that if disturbances are uniform the transient resistive losses are a monotonically decreasing function of the active power droop gains regardless of network topology. On the other hand, these losses depend on both the reactive power droop gains and the network topology due to the voltage dynamics. Numerical examples further analyzing the losses reveal that they can be amplified by high droop gain heterogeneity. These simulations also provide insights into how non-uniform line susceptances affect judicious selection of the droop gains for decreasing the losses.

H. G. Oral and D. F. Gayme are with the Department of Mechanical Engineering at The Johns Hopkins University, Baltimore, MD, USA, 21218. giray@jhu.edu, dennice@jhu.edu. Partial support by the NSF (CNS 1544771) is gratefully acknowledged.

The remainder of the paper is organized as follows. Section II describes the system model, performance measures and the structural assumptions undertaken. Section III provides our main results characterizing the system performance based on total transient frequency and voltage deviations as well as resistive losses. Section IV provides numerical examples. Section V concludes the paper.

II. Problem Formulation

A. Linearized Model of the Microgrid Dynamics

We adopt the framework in [5], [10] and consider a Kron-reduced network [20] of inverters over a weighted, undirected, and connected graph $\mathcal{G} = \{\mathcal{N}, \mathcal{E}\}$. Here $\mathcal{N} = \{1, ..., N\}$ is the set of nodes representing the inverters and $\mathcal{E} = \{\mathcal{E}_{ik}\}$ is the set of edges representing the lines.

The active and reactive power injections P_i and Q_i into the network at node i are given by

$$P_i = -g_{ii}V_i^2 + \sum_{i\sim k} g_{ik}V_iV_k\cos\theta_{ik} + b_{ik}V_iV_k\sin\theta_{ik}, \quad (1a)$$

$$Q_i = b_{ii}V_i^2 + \sum_{i\sim k} g_{ik}V_iV_k\sin\theta_{ik} - b_{ik}V_iV_k\cos\theta_{ik}, \quad (1b)$$

where V_i and θ_i are the respective nodal voltage magnitude and phase angle and $\theta_{ik} := \theta_i - \theta_k$ if $i \sim k$ (i.e. $\mathcal{E}_{ik} \in \mathcal{E}$). The conductance and susceptance of each line are respectively denoted by $g_{ik}, b_{ik} > 0$. Here $g_{ii} = \bar{g}_i + \sum_{i\sim k} g_{ik}$, and $b_{ii} = \bar{b}_i + \sum_{i\sim k} b_{ik}$ with shunt conductance and susceptance $\bar{g}_i$ and $\bar{b}_i$, respectively. We assume that shunt elements are purely inductive [6], i.e. $\bar{g}_i = 0$, and $\bar{b}_i \geq 0$. Assuming small deviations from the equilibrium, the first-order Taylor series expansions of (1a) and (1b) around $(V_i^* = V_k^* = 1, \theta_{ik}^* = 0)$ lead to

$$\Delta P_i \approx \sum_{i\sim k} \left(b_{ik}\Delta\theta_{ik} - g_{ik}(\Delta V_i - \Delta V_k)\right), \quad (2a)$$

$$\Delta Q_i \approx 2\bar{b}_i\Delta V_i + \sum_{i\sim k} \left(g_{ik}\Delta\theta_{ik} + b_{ik}(\Delta V_i - \Delta V_k)\right), \quad (2b)$$

where the 'Δ' terms indicate the deviation of the respective variable from its equilibrium value. In the following, by an abuse of notation we omit the 'Δ' from these variables.

Remark 1: By the choice of $\theta_{ik}^* = 0$ we assume that the phase angle differences are small at equilibrium, which is a common assumption in power systems analysis [8], [10].

Droop control aims to operate each inverter at a common frequency ω^* and attain the desired nodal voltage magnitude V_i^*, active power P_i^* and reactive power Q_i^* via the following control laws [2]:

$$\omega_i = \omega^* - k_{P_i}(\hat{P}_i - P_i^*), \quad V_i = V_i^* - k_{Q_i}(\hat{Q}_i - Q_i^*), \quad (3)$$

where ω_i is the frequency, $\hat{P}_i$ and $\hat{Q}_i$ are the respective active and reactive power measurements, and $k_{P_i} > 0$ and $k_{Q_i} > 0$ are the active and reactive power droop gains at node i. We assume that the power measurements are governed by first order dynamics [10] with time constants τ_{P_i}, τ_{Q_i}. Differentiating (3) with respect to time gives the following closed-loop dynamics at each node i

$$\dot{\theta}_i = \omega_i, \quad \tau_{P_i}\dot{\omega}_i = -\omega_i + \omega^* - k_{P_i}(P_i - P_i^*), \quad (4a)$$

$$\tau_{Q_i}\dot{V}_i = -V_i + V_i^* - k_{Q_i}(Q_i - Q_i^*). \quad (4b)$$

Using equations (2), (4) and introducing the disturbance input w, the closed-loop dynamics can be written as

$$\dot{x} = Ax + B\mathrm{w}, \quad (5)$$

where $x := \begin{bmatrix}\theta^T & \omega^T & V^T\end{bmatrix}^T$, $\mathrm{w} := \begin{bmatrix}(\mathrm{w}^P)^T & (\mathrm{w}^Q)^T\end{bmatrix}^T$,

$$A := \begin{bmatrix} 0 & I & 0 \\ -T_P^{-1}K_PL_B & -T_P^{-1} & T_P^{-1}K_PL_G \\ -T_Q^{-1}K_QL_G & 0 & -T_Q^{-1}(C_Q + K_QL_B)\end{bmatrix},$$

$B := \begin{bmatrix}0 & T_P^{-1} & 0 \\ 0 & 0 & T_Q^{-1}\end{bmatrix}^T$, $K_P := \mathrm{diag}\{k_{P_i}\}$, $K_Q := \mathrm{diag}\{k_{Q_i}\}$, $T_P := \mathrm{diag}\{\tau_{P_i}\}$, $T_Q := \mathrm{diag}\{\tau_{Q_i}\}$, $C_Q = \mathrm{diag}\{c_{Q_i}\}$. Here, $\mathrm{diag}\{\cdot\}$ denotes the diagonal matrix of the scalars in its argument and $c_{Q_i} = 1 + 2\bar{b}_ik_{Q_i}$. We define the weighted Laplacian matrix L_B as: $[L_B]_{ii} := \sum_{i\sim k} b_{ik}$, $[L_B]_{ik} := -b_{ik}$ if $i \sim k$, $[L_B]_{ik} := 0$ otherwise. L_G is defined similarly using the conductances g_{ik}. The eigenvalues of L_B are denoted by $0 = \lambda_1 < \lambda_2 \leq \cdots \leq \lambda_N$.

We will evaluate the system performance in the presence of a distributed impulse disturbance input of the form

$$\mathrm{w}(t) = \delta(t)\mathrm{w}_0, \quad (6)$$

where $\delta(t)$ denotes the Dirac delta function and $\mathrm{w}_0 \in \mathbb{R}^N$ defines the input magnitude and direction.

Remark 2: The special case of (6) in which $E\{\mathrm{w}_0\mathrm{w}_0^T\} = I$ is equivalent to a white noise input $u(t)$ with unit covariance, i.e. $E\{u(0)u(t)^T\} = \delta(t)I$, which naturally arises in $\mathcal{H}_2$ norm based analysis [8]. Therefore, (6) is a generalization that can model spatially correlated disturbance inputs.

B. Performance Measures

In this section we introduce the two performance measures that are the subject of this work; the total transient deviation from frequency and voltage synchrony, and the total transient resistive power losses. The former is a measure of the efficiency of system synchronization in the presence of disturbances while the latter can be interpreted as the "cost" of this synchronization.

1) Deviation from Synchrony: In the following analysis we will show that the frequency can be decomposed as

$$\omega(t) = \bar{\omega}(t)\mathbf{1} + \tilde{\omega}(t)$$

in analogy with transmission networks [18], where $\bar{\omega}(t) \in \mathbb{R}$ denotes the synchronous system frequency and $\tilde{\omega}(t) \in \mathbb{R}^N$ denotes deviations from it. As discussed later, a similar decomposition is not always possible for $V(t)$ if the inverter ratings are heterogeneous, therefore we consider voltage deviations from the equilibrium. For the sake of simplicity, we also use the term "synchrony" for the voltage dynamics by an abuse of terminology. Combining these ideas the total transient deviation from synchrony can be quantified by

$$\Pi_{sync} = \int_0^\infty \|\tilde{\omega}(t)\|_2^2 dt + \int_0^\infty \|V(t)\|_2^2 dt =: \|y_{sync}\|_{\mathcal{L}_2}^2, \quad (7)$$

where $y_{sync} := \begin{bmatrix}\tilde{\omega}^T & V^T\end{bmatrix}^T$ defines the performance output and $\|\cdot\|_2$ denotes the Euclidean norm. The frequency part of

the measure in (7) was used in [18] to quantify the deviations from synchrony in a transmission network with heterogeneous generator inertia, subjected to step disturbances.

2) Transient Resistive Power Losses: The instantaneous resistive power loss incurred across each line $\mathcal{E}_{ik}$ is

$$\Pi_{ik}^{loss} = g_{ik}|v_i - v_k|^2, \tag{8}$$

where $v_i = V_i e^{\mathbf{j}\theta_i}$ is the complex voltage. Using standard trigonometric identities (8) becomes $\Pi_{ik}^{loss} = g_{ik}(V_i^2 + V_k^2 - 2V_iV_k\cos\theta_{ik})$. A second order Taylor series expansion around $(V_i^* = V_k^* = 1, \theta_{ik}^* = 0)$ leads to

$$\Pi_{ik}^{loss} \approx g_{ik}[(V_i - V_k)^2 + (\theta_i - \theta_k)^2]. \tag{9}$$

The corresponding total transient resistive power losses are given by $\Pi_{loss} = \int_0^\infty \sum_{i\sim k} \Pi_{ik}^{loss}(t)dt$. Using (9) and re-writing this expression in terms of L_G gives

$$\Pi_{loss} \approx \int_0^\infty \big[V(t)^T L_G V(t) + \theta(t)^T L_G \theta(t)\big]dt = \|y_{loss}\|_{\mathcal{L}_2}^2, \tag{10}$$

where the output, $y_{loss} := \begin{bmatrix} L_G^{\frac{1}{2}} & 0 & 0 \\ 0 & 0 & L_G^{\frac{1}{2}} \end{bmatrix} x.$

C. Decoupled Dynamics for Performance Analysis

We will employ the following assumptions from [10], which are common in power system performance analysis.

Assumption 1: The power measurement time constants τ_{P_i} and τ_{Q_i} are uniform across all inverters, i.e. $\tau_{P_i} = \tau_P$ and $\tau_{Q_i} = \tau_Q \ \forall i \in \mathcal{N}$.

Assumption 2: Shunt susceptances are uniform across all nodes, i.e. $\bar{b}_i = \bar{b} \ \forall i \in \mathcal{N}$.

Assumption 3: The conductance-to-susceptance ratio α is uniform for all edges, i.e. $\alpha := \frac{g_{ik}}{b_{ik}} \ \forall \mathcal{E}_{ik}$.

Assumption 4: The transmission lines are inductive, i.e. the conductance-to-susceptance (resistance-to-reactance) ratio α is small, $\alpha \approx 0$.

Remark 3: Assumption 3 is reasonable in this setting due to the increased uniformity in node degrees in Kron-reduced networks [22] and the uniformity of physical line properties in microgrids. Although Assumption 4 is not applicable in general, it is reasonable for an inverter-based network since inverter output impedances are highly inductive [6] and can dominate line resistances in a Kron-reduced model. Although the analysis easily extends to the case of non-uniform shunt susceptances, we use Assumption 2 for notational simplicity.

Assumtion 3 implies that $L_G = \alpha L_B$ which is then combined with assumptions 1, 2 and 4 so that (5) leads to the decoupled phase-frequency and voltage dynamics

$$\begin{bmatrix} \dot{\theta} \\ \dot{\omega} \\ \dot{V} \end{bmatrix} = \begin{bmatrix} 0 & I & 0 \\ -\frac{1}{\tau_P}K_P L_B & -\frac{1}{\tau_P}I & 0 \\ 0 & 0 & -\frac{1}{\tau_Q}(C_Q + K_Q L_B) \end{bmatrix} \begin{bmatrix} \theta \\ \omega \\ V \end{bmatrix} + \\ + \begin{bmatrix} 0 & 0 \\ \frac{1}{\tau_P}I & 0 \\ 0 & \frac{1}{\tau_Q}I \end{bmatrix} \mathrm{w}, \ y_{loss} = \sqrt{\alpha} \begin{bmatrix} L_B^{\frac{1}{2}}\theta \\ L_B^{\frac{1}{2}}V \end{bmatrix}, \ y_{sync} = \begin{bmatrix} \tilde{\omega} \\ V \end{bmatrix}. \tag{11}$$

This decoupling between phase and voltage as well as frequency and voltage will enable us to quantify the individual contributions of frequency and voltage dynamics to the performance measures in (7) and (10).

III. Performance of Heterogeneously Rated Inverters

In this section, we employ the framework introduced in [18] to investigate the effect of heterogeneous inverter ratings on the performance of droop-controlled microgrids.

A. Diagonalization of the Closed-Loop System

We begin by defining a parameter called the node rating. When considering frequency and voltage dynamics individually we respectively choose the node ratings as $f_{P_i} := \frac{k_{P_i}}{k_P}$ and $f_{Q_i} := \frac{k_{Q_i}}{k_Q}$ for $i = 1, \ldots, N$ such that they determine the ratio of each droop gain to predetermined constants $k_P > 0$ and $k_Q > 0$.

By taking the Laplace transform of (4) and excluding the power flow terms, we define two open-loop transfer functions associated with each node; one corresponding to the phase and the other to the voltage dynamics

$$g_i^P(s) := \frac{k_{P_i}}{\tau_P s^2 + s} \ \text{ and } \ g_i^Q(s) := \frac{k_{Q_i}}{\tau_Q s + 1}, \ \ i = 1, \ldots, N.$$

These can be written in terms of the node ratings as

$$g_i^P(s) = f_{P_i} g_0^P(s) \ \text{ and } \ g_i^Q(s) = f_{Q_i} g_0^Q(s), \ \ i = 1, \ldots, N,$$

where $g_0^P(s)$ and $g_0^Q(s)$ are node-independent reference transfer functions with fixed parameters (independent of k_{P_i} or k_{Q_i}). We specify these reference transfer functions as

$$g_0^P(s) = \frac{k_P}{\tau_P s^2 + s} \ \text{ and } \ g_0^Q(s) = \frac{k_Q}{\tau_Q s + 1}.$$

Combining the nodal open-loop transfer functions leads to the open-loop transfer function of the system

$$\mathcal{G}(s) := \begin{bmatrix} \mathrm{diag}\{g_i^P(s)\} & \\ & \mathrm{diag}\{g_i^Q(s)\} \end{bmatrix} = \mathcal{F} g(s), \tag{12}$$

where $\mathcal{F} := \begin{bmatrix} F_P & \\ & F_Q \end{bmatrix}$, $F_P := \mathrm{diag}\{f_{P_i}\}$, $F_Q := \mathrm{diag}\{f_{Q_i}\}$ and $g(s) := \begin{bmatrix} g_0^P(s)I & \\ & g_0^Q(s)I \end{bmatrix}$.

Based on the state equation in (11), the closed loop system is given by the block diagram in Figure 1. Here, we introduce the feedback matrix

$$\mathcal{L} := \begin{bmatrix} L_B & \\ & 2\bar{b}I + L_B \end{bmatrix},$$

which determines the power flows emerging from the underlying interconnection graph; as well as the matrix of droop gains $\mathcal{K} := \begin{bmatrix} K_P & \\ & K_Q \end{bmatrix}$. Due to (12), $\mathcal{G}(s) = \mathcal{F}^{\frac{1}{2}} g(s) \mathcal{F}^{\frac{1}{2}}$

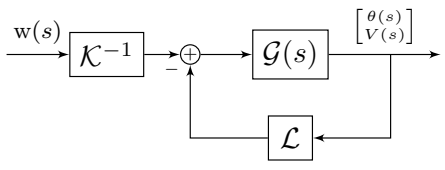

Fig. 1: Closed-loop microgrid dynamics.

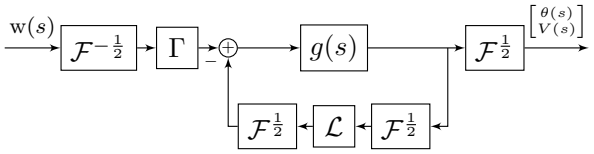

Fig. 2: Closed-loop dynamics with the open-loop determined by the reference transfer functions and the scaled Laplacians in the feedback.

which along with block manipulations leads to the block diagram in Figure 2, where $\Gamma := \begin{bmatrix} \frac{1}{k_P} I & \\ & \frac{1}{k_Q} I \end{bmatrix}$. We use a scaled Laplacian [18] defined by

$$\mathcal{L}_{\mathcal{F}} := \mathcal{F}^{\frac{1}{2}} \mathcal{L} \mathcal{F}^{\frac{1}{2}} = \begin{bmatrix} F_P^{\frac{1}{2}} L_B F_P^{\frac{1}{2}} & \\ & F_Q^{\frac{1}{2}} (2\bar{b} I + L_B) F_Q^{\frac{1}{2}} \end{bmatrix}, \quad (13)$$

which is symmetric, therefore orthogonally diagonalizable

$$\mathcal{L}_{\mathcal{F}} := \mathcal{S} \Lambda \mathcal{S}^T, \quad (14)$$

where $\mathcal{S} \in \mathbb{R}^{N \times N}$ and $\mathcal{S}\mathcal{S}^T = I$, and $\Lambda \in \mathbb{R}^{N \times N}$ is diagonal. Due to the block diagonal form of (13), the decomposition in (14) is also block diagonal with

$$\mathcal{S} = \begin{bmatrix} R & \\ & U \end{bmatrix} \quad \text{and} \quad \Lambda = \begin{bmatrix} \Lambda_P & \\ & \Lambda_Q \end{bmatrix},$$

which equivalently results in the orthogonal diagonalizations

$$\mathcal{L}_{\mathcal{F}} =: \begin{bmatrix} L_P & \\ & L_Q \end{bmatrix} = \begin{bmatrix} R \Lambda_P R^T & \\ & U \Lambda_Q U^T \end{bmatrix}. \quad (15)$$

This decomposition and block manipulations lead to the diagonalized closed-loop dynamics shown in the block diagram of Figure 3 with the transfer function

$$T(s) = \mathcal{F}^{\frac{1}{2}} \mathcal{S} H(s) \mathcal{S}^T \mathcal{F}^{-\frac{1}{2}}.$$

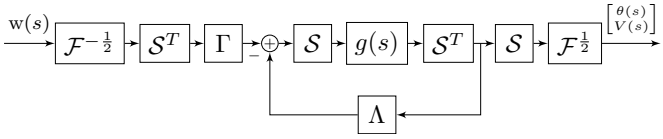

Fig. 3: Diagonalized Closed-loop dynamics.

The diagonalized transfer function $H(s)$ can be partitioned with respect to phase-frequency and voltage dynamics as

$$H(s) = \begin{bmatrix} H^P(s) & \\ & H^Q(s) \end{bmatrix}.$$

We next describe each of these blocks.

1) Phase-Frequency Dynamics: Since F_P is full rank, L_P is positive semi-definite and rank $N-1$ due to (13). Therefore the decomposition in (15) leads to $\Lambda_P =: \operatorname{diag}\{\lambda_i^P\}$ and $0 = \lambda_1^P < \lambda_2^P \leq \cdots \leq \lambda_N^P$.

The transfer function from $\mathrm{w}^P(s)$ to $\theta(s)$ in Figure 3 is

$$T_{\theta \mathrm{w}^P}(s) = F_P^{\frac{1}{2}} R H^P(s) R^T F_P^{-\frac{1}{2}}, \quad (16)$$

where $H^P(s) = \operatorname{diag}\{h_i^P(s)\}$ and for $i = 1, \ldots, N$,

$$h_i^P(s) = \frac{1}{k_P} \left(\frac{g_0^P(s)}{1 + \lambda_i^P g_0^P(s)} \right) = \frac{1}{\tau_P s^2 + s + \lambda_i^P k_P}. \quad (17)$$

Given the partition $R = \begin{bmatrix} r_1 & R_\perp \end{bmatrix}$, the first eigenvector of L_P can be written as $r_1 = \gamma_P F_P^{-\frac{1}{2}} \mathbf{1}$, with the normalization parameter $\gamma_P = \left(\sum_{i=1}^N f_{P_i}^{-1} \right)^{-\frac{1}{2}}$ and $\mathbf{1} = \begin{bmatrix} 1 \ \ldots \ 1 \end{bmatrix}^T$. Using (16), the phase signal due to input (6) is given by

$$\begin{aligned} \theta(s) &=: \bar{\theta}(s) \mathbf{1} + \tilde{\theta}(s) \quad (18) \\ &= \underbrace{F_P^{\frac{1}{2}} r_1}_{= \gamma_P \mathbf{1}} h_1^P(s) r_1^T F_P^{-\frac{1}{2}} \mathrm{w}_0^P + F_P^{\frac{1}{2}} R_\perp \tilde{H}^P(s) R_\perp^T F_P^{-\frac{1}{2}} \mathrm{w}_0^P, \end{aligned}$$

where $R_\perp = \begin{bmatrix} r_2 \ \ldots \ r_N \end{bmatrix}$, $\tilde{H}^P(s) := \operatorname{diag}\{h_i^P(s)\}_{i=2,\ldots,N}$. We note that the frequency signal can be obtained from

$$\omega(s) = s\theta(s) =: \bar{\omega}(s) \mathbf{1} + \tilde{\omega}(s), \quad (19)$$

which is characterized by the dynamic terms

$$h_i^{P,\omega}(s) := s h_i^P(s), \quad i = 1, \ldots, N. \quad (20)$$

Since $r_1^T R_\perp = 0$, we have $\mathbf{1}^T F_P^{-1} \tilde{\omega}(s) = 0$. Then multiplying the equation above from the left by $\mathbf{1}^T F_P^{-1}$ leads to the expression for the synchronous frequency $\bar{\omega}(t)$

$$\bar{\omega}(t) = \frac{\sum_{i=1}^N f_{P_i}^{-1} \omega_i(t)}{\sum_{i=1}^N f_{P_i}^{-1}} = \frac{\sum_{i=1}^N k_{P_i}^{-1} \omega_i(t)}{\sum_{i=1}^N k_{P_i}^{-1}}.$$

This is analogous to the center of inertia (COI) in transmission networks [18] in the sense that the averaging weights are the inverses of active power droop gains instead of inertias.

The following result proves the stability of the phase-frequency dynamics.

Proposition 1: The phase and frequency deviations $\tilde{\theta}(t)$ and $\tilde{\omega}(t)$ are asymptotically stable.

Proof: First, observe from (18) and (19) that the stability of $\tilde{\theta}$ and $\tilde{\omega}$ are respectively determined by $h_i^P(s)$ and $h_i^{P,\omega}(s)$ for $i = 2, \ldots, N$. Then the result follows from (17) and (20) by noting that $\lambda_i^P > 0$ for $i = 2, \ldots, N$. ■

2) Voltage Dynamics: Since F_Q is full rank, L_Q is positive definite and full rank due to (13). Therefore the decomposition in (15) leads to $\Lambda_Q = \operatorname{diag}\{\lambda_i^Q\}$ and $0 < \lambda_1^Q \leq \lambda_2^Q \leq \cdots \leq \lambda_N^Q$.

The transfer function from $\mathrm{w}^Q(s)$ to $V(s)$ in Figure 3 is

$$T_{V \mathrm{w}^Q}(s) = F_Q^{\frac{1}{2}} U H^Q(s) U^T F_Q^{-\frac{1}{2}}, \quad (21)$$

where $U = \begin{bmatrix} u_1 \ \ldots \ u_N \end{bmatrix}$, $H^Q(s) = \operatorname{diag}\{h_i^Q(s)\}$ and

$$h_i^Q(s) = \frac{1}{k_Q} \left(\frac{g_0^Q(s)}{1 + \lambda_i^Q g_0^Q(s)} \right) = \frac{1}{\tau_Q s + \lambda_i^Q k_Q + 1}, \quad (22)$$

for $i = 1, \ldots, N$. Using (21) the voltage due to input (6) is

$$V(s) = F_Q^{\frac{1}{2}} U H^Q(s) U^T F_Q^{-\frac{1}{2}} \mathrm{w}_0^Q = \sum_{i=1}^N h_i^Q(s) \xi_i, \quad (23)$$

where $\xi_i = \left(u_i^T F_Q^{-\frac{1}{2}} \mathrm{w}_0^Q \right) F_Q^{\frac{1}{2}} u_i \in \mathbb{R}^N$. In contrast to the frequency in (19), the voltage signal may not include an inherent synchronous mode characterized by $\mathbf{1}$ if the reactive power droop gains are heterogeneous. This is shown in Proposition 2 and for this reason we consider the deviations from the equilibrium voltage as defined by (7).

Proposition 2: Suppose that u_i has non-zero entries for all i such that $\xi_i \neq 0$. If $F_Q \neq \zeta I$ for all $\zeta > 0$, then $\xi_i \notin \operatorname{span}\{\mathbf{1}\}$ for all i such that $\xi_i \neq 0$.

Proof: Using (23) consider $\xi_i = \left(u_i^T F_Q^{-\frac{1}{2}} \mathrm{w}_0^Q\right) F_Q^{\frac{1}{2}} u_i \neq 0$. Assume that $\xi_i \equiv \beta_i \mathbf{1}$ and $0 \neq \beta_i \in \mathbb{R}$ for some i such that $\xi_i \neq 0$. Then noting that $u_i = \eta_i F_Q^{-\frac{1}{2}} \mathbf{1}$ for $0 \neq \eta_i \in \mathbb{R}$, we have $\lambda_i^Q u_i = L_Q u_i = \eta_i F_Q^{\frac{1}{2}} (2\bar{b} I + L_B)\mathbf{1} = 2\bar{b} F_Q u_i$, where we used (13) and (15). This implies that $F_Q = \frac{\lambda_i^Q}{2\bar{b}} I$ since by assumption u_i has non-zero entries. ∎

The following result proves the stability of the voltage dynamics.

Proposition 3: The voltage $V(t)$ is asymptotically stable.

Proof: The result follows from (22) and (23) by noting that $\lambda_i^Q > 0$ for $i = 1, \ldots, N$. ∎

Next we study the deviations from synchrony.

B. Deviation from Synchrony

In this subsection, we study the synchronization performance of (11). The following lemma provides a preliminary result that will be used in the analysis that follows.

Lemma 1: The measure Π_{sync} in (7) is given by

$$\Pi_{sync} \;=\; z_0^T \Psi z_0,$$

where $z_0 := \begin{bmatrix}(z_0^P)^T & (z_0^Q)^T\end{bmatrix}^T$, $z_0^P = R_\perp^T F_P^{-\frac{1}{2}} \mathrm{w}_0^P$ and $z_0^Q = U^T F_Q^{-\frac{1}{2}} \mathrm{w}_0^Q$. The matrix $\Psi := \begin{bmatrix}\Psi^P & \\ & \Psi^Q\end{bmatrix}$ has the entries

$$\psi_{ij}^P \;=\; \phi_{ij}^P \langle h_{i+1}^{P,\omega}, h_{j+1}^{P,\omega}\rangle, \quad i,j = 1,\ldots,N-1, \tag{24}$$

$$\psi_{ij}^Q \;=\; \phi_{ij}^Q \langle h_i^Q, h_j^Q\rangle, \qquad i,j = 1,\ldots,N, \tag{25}$$

where ϕ_{ij}^P and ϕ_{ij}^Q respectively denote the entries of $\Phi^P := R_\perp^T F_P R_\perp$ and $\Phi^Q := U^T F_Q U$. The inner products in (24) and (25) are given by

$$\langle h_i^{P,\omega}, h_j^{P,\omega}\rangle \;=\; \frac{\lambda_i^P + \lambda_j^P}{2\tau_P(\lambda_i^P + \lambda_j^P) + k_P \tau_P^2 (\lambda_i^P - \lambda_j^P)^2}, \tag{26}$$

$$\langle h_i^Q, h_j^Q\rangle \;=\; \frac{1}{2\tau_Q + k_Q \tau_Q (\lambda_i^Q + \lambda_j^Q)}. \tag{27}$$

Proof: See Appendix. ∎

Note that Π_{sync} depends on the heterogeneous droop gains through the eigenvalues λ_i^P and λ_i^Q. Lemma 1 is next used to compute Π_{sync} for homogeneous inverter ratings.

Theorem 1 (Homogeneous Inverter Ratings): Suppose that $\mathcal{F} = I$. Then Π_{sync} in (7) is given by

$$\Pi_{sync} \;=\; \frac{1}{2\tau_P}\sum_{i=2}^{N} (r_i^T \mathrm{w}_0^P)^2 \;+\; \frac{1}{2\tau_Q}\sum_{i=1}^{N} \frac{(u_i^T \mathrm{w}_0^Q)^2}{c_Q + k_Q \lambda_i},$$

where $c_Q = 1 + 2\bar{b} k_Q$. If in addition $E\{\mathrm{w}_0 \mathrm{w}_0^T\} = I$, then

$$E\{\Pi_{sync}\} \;=\; \frac{1}{2\tau_P}(N-1) \;+\; \frac{1}{2\tau_Q}\sum_{i=1}^{N} \frac{1}{c_Q + k_Q \lambda_i}.$$

Proof: $F_P = F_Q = I$ leads to $\Phi^P = I$ and $\Phi^Q = I$ so Ψ_P and Ψ_Q are diagonal due to (24), (25). Also $z_0^P = R_\perp^T \mathrm{w}_0^P$ and $z_0^Q = U^T \mathrm{w}_0^Q$. Using Lemma 1, $\Pi_{sync} = \mathrm{tr}(z_0 z_0^T \Psi)$ which yields the first result via (26), (27). Assuming $E\{\mathrm{w}_0 \mathrm{w}_0^T\} = I$, the second result follows from $E\{(r_i^T \mathrm{w}_0^P)^2\} = E\{r_i^T \mathrm{w}_0^P (\mathrm{w}_0^P)^T r_i\} = 1$ and $E\{(u_i^T \mathrm{w}_0^Q)^2\} = 1$. ∎

If the disturbances have unit covariance and the inverter ratings are homogeneous, the contribution of frequency dynamics is independent of network topology whereas that of the voltage dynamics depends on the topology through the eigenvalues of L_B. If the disturbance direction is arbitrary, then for given $\|\mathrm{w}_0^P\|_2$, the contribution of frequency dynamics is zero if $\mathrm{w}_0^P \in \mathrm{span}\{\mathbf{1}\}$ and maximal if $\mathrm{w}_0^P \in \mathrm{span}\{\mathbf{1}\}^\perp$ since in the homogeneous case $r_1 = \frac{1}{\sqrt{N}}\mathbf{1}$. Similarly for given $\|\mathrm{w}_0^Q\|_2$, the contribution of voltage dynamics is minimal if $\mathrm{w}_0^Q \in \mathrm{span}\{u_N\}$ and maximal if $\mathrm{w}_0^Q \in \mathrm{span}\{\mathbf{1}\}$.

The next theorem provides an analogous result for heterogeneous inverter ratings.

Theorem 2 (Heterogeneous Inverter Ratings): For given inverter ratings $\mathcal{F}$, Π_{sync} in (7) has the asymptotic value

$$\Pi_{sync} \;\to\; \frac{1}{2\tau_P}\sum_{i=1}^{N-1} \phi_{ii}^P (z_{0i}^P)^2,$$

assuming that $\lambda_i^P \neq \lambda_j^P$ for $i \neq j$, as $k_P \to \infty$ and $k_Q \to \infty$, i.e. in the limit of large droop gains; and

$$\Pi_{sync} \;\to\; \frac{1}{2\tau_P}\sum_{i,j=1}^{N-1} \phi_{ij}^P z_{0i}^P z_{0j}^P \;+\; \frac{1}{2\tau_Q}\sum_{i,j=1}^{N} \phi_{ij}^Q z_{0i}^Q z_{0j}^Q,$$

as $k_P \to 0$ and $k_Q \to 0$, i.e. in the limit of small gains.

Proof: In the limit of $k_P \to \infty$ and $k_Q \to \infty$, (24) and (25) lead to the fact that Ψ^P is diagonal with $\psi_{ii}^P \to \frac{\phi_{ii}^P}{2\tau_P}$ and $\Psi^Q \to 0$. Similarly, as $k_P \to 0$ and $k_Q \to 0$, $\psi_{ij}^P \to \frac{\phi_{ij}^P}{2\tau_P}$ and $\psi_{ij}^Q \to \frac{\phi_{ij}^Q}{2\tau_Q}$. Using the fact from Lemma 1 that $\Pi_{sync} = \mathrm{tr}(z_0 z_0^T \Psi)$ yields the result. ∎

In these asymptotic expressions the dependence on heterogeneous droop gains is through the entries of Φ^P, Φ^Q and z_0. The dependence on network topology is only through the eigenvectors r_i and u_i of the scaled Laplacians L_P and L_Q; and λ_i^P and λ_i^Q do not appear. For given F_P and F_Q, Π_{sync} in the small gain limit has additional summation terms for $i \neq j$, while these terms are suppressed in the large gain limit. Furthermore, in the limit of large gains there is no deviation from the equilibrium voltage hence the contribution of the voltage dynamics to Π_{sync} is zero. In contrast, frequency deviations cannot be eliminated even with infinite control action. Theorem 2 therefore shows that lack of inertia can indeed be problematic in inverter-based systems because even at the large gain limit frequency deviations can grow unboundedly as the disturbance magnitude is increased. Additional inertia would contribute to the time constant term τ_P due to (4), and help to mitigate these deviations. Dynamic control strategies can also improve frequency synchronization [17].

C. Transient Resistive Power Losses

In this subsection, we begin by providing the closed-form solution for the transient resistive losses. In the special cases where disturbance directions have unit covariance and the covariance scales with inverter ratings, we will analyze the dependence of losses on the droop gains k_{P_i} and k_{Q_i}.

Lemma 2: The measure Π_{loss} in (10) is given by

$$\Pi_{loss} \;=\; \underbrace{\frac{\alpha}{2k_P}\sum_{i=1}^{N-1}\left(z_{0i}^{P}\right)^2}_{=:\,\Pi_{loss}^{P}} \;+\; \underbrace{\frac{\alpha}{2\tau_Q}\sum_{i=1}^{N}\frac{\left(z_{0i}^{Q}\right)^2}{k_Q+\frac{1}{\lambda_i^Q}}}_{=:\,\Pi_{loss}^{Q}} \;-\; \Sigma^Q$$

where the notation is adopted from Lemma 1 and

$$\Sigma^Q \;=\; 2\alpha\bar{b}(z_0^Q)^T\Psi_Q z_0^Q. \tag{28}$$

Furthermore $\Pi_{loss}\to 0$ as $k_P\;\to\;\infty$ and $k_Q\to\infty$, i.e. in the limit of large droop gains for given inverter ratings $\mathcal{F}$.

Proof: See Appendix. ∎

As Lemma 2 indicates, Π_{loss} depends on both the droop gains and the network topology. The dependence on network topology is through the eigenvectors r_i and u_i of the scaled Laplacian for Π_{loss}^P whereas Π_{loss}^Q additionally includes the eigenvalues λ_i^Q. Note that these variables also are functions of the droop gains. Π_{loss} can be eliminated in the hypothetical case of infinite gains, while this is not true for Π_{sync} as shown by theorems 1 and 2.

We now investigate the effect of network topology and heterogeneous droop gains on the transient resistive losses.

Theorem 3: Suppose that $E\{\mathrm{w}_0\mathrm{w}_0^T\}=I$. Then

$$E\{\Pi_{loss}\} \;=\; \frac{\alpha}{2}\left(\sum_{i=1}^{N}k_{P_i}^{-1}-\frac{\sum_{i=1}^{N}k_{P_i}^{-2}}{\sum_{i=1}^{N}k_{P_i}^{-1}}\right) + \frac{\alpha}{2\tau_Q}\sum_{i=1}^{N}\frac{u_i^TF_Q^{-1}u_i}{k_Q+\frac{1}{\lambda_i^Q}} \;-\; E\{\Sigma^Q\},$$

where Σ^Q is given by (28). If $E\{\mathrm{w}_0\mathrm{w}_0^T\}=\mathcal{F}$, then

$$E\{\Pi_{loss}\} \;=\; \frac{\alpha}{2k_P}(N-1) \;+\; \frac{\alpha}{2\tau_Q}\sum_{i=1}^{N}\frac{\lambda_i^Q-2\bar{b}u_i^TF_Qu_i}{1+k_Q\lambda_i^Q}.$$

Proof: Assuming $E\{\mathrm{w}_0\mathrm{w}_0^T\}=I$, we have $E\{(z_{0i}^P)^2\}=r_{i+1}^TF_P^{-1}r_{i+1}$ and $E\{(z_{0i}^Q)^2\}=u_i^TF_Q^{-1}u_i$. Then using $E\{\Pi_{loss}^P\}=\frac{\alpha}{2k_P}\mathrm{tr}\big(R_\perp R_\perp^TF_P^{-1}\big)=\frac{\alpha}{2k_P}\mathrm{tr}\big[\big(I-r_1r_1^T\big)F_P^{-1}\big]$ and recalling that $r_1=\gamma_PF_P^{-\frac{1}{2}}\mathbf{1}$ and $\gamma_P=\left(\sum_{i=1}^N f_{P_i}^{-1}\right)^{-\frac{1}{2}}$ leads to

$$\begin{aligned}E\{\Pi_{loss}^P\} &= \frac{\alpha}{2k_P}\,\mathrm{tr}\left(F_P^{-1}-\gamma_P^2F_P^{-1}\mathbf{1}\mathbf{1}^TF_P^{-1}\right)\\ &= \frac{\alpha}{2k_P}\left(\sum_{i=1}^{N}f_{P_i}^{-1}-\frac{\sum_{i=1}^{N}f_{P_i}^{-2}}{\sum_{i=1}^{N}f_{P_i}^{-1}}\right).\end{aligned}$$

Taking $\frac{1}{k_P}$ inside the parenthesis yields the first result. Assuming that $E\{\mathrm{w}_0\mathrm{w}_0^T\}=\mathcal{F}$, we have $E\{z_0^P(z_0^P)^T\}=I$ and $E\{z_0^Q(z_0^Q)^T\}=I$. Therefore (25) and (28) lead to

$$E\{\Sigma^Q\} \;=\; 2\alpha\bar{b}\,\mathrm{tr}\,(\Psi_Q) \;=\; 2\alpha\bar{b}\sum_{i=1}^{N}u_i^TF_Qu_i\|h_i^Q(t)\|_{\mathcal{L}_2}^2.$$

Combining (33) and Lemma 2 completes the proof. ∎

If the disturbance has unit covariance, $E\{\Pi_{loss}^P\}$ only depends on the active power droop gains and is independent of network topology. In contrast, $E\{\Pi_{loss}^Q\}$ depends on the reactive power droop gains as well as the network topology. Scaling the inverter ratings in accordance with the disturbance magnitude at each node leads to $E\{\Pi_{loss}^P\}$ scaling linearly with network size, while $E\{\Pi_{loss}^Q\}$ still depends both on network topology and droop gains.

Next we show $E\{\Pi_{loss}^P\}$ is monotonically decreasing in the active power droop gains if the disturbance has unit covariance.

Corollary 1: If $E\{\mathrm{w}_0\mathrm{w}_0^T\}=I$, then $E\{\Pi_{loss}^P\}$ is monotonically decreasing in k_{P_l} for $l=1,\ldots,N$, i.e.

$$\frac{\partial}{\partial k_{P_l}}\left[\frac{\alpha}{2}\left(\sum_{i=1}^{N}k_{P_i}^{-1}-\frac{\sum_{i=1}^{N}k_{P_i}^{-2}}{\sum_{i=1}^{N}k_{P_i}^{-1}}\right)\right]<0,\quad l=1,\ldots,N.$$

Proof: See Appendix. ∎

Since the derivative in each direction is negative, performance is improved by increasing any of the active power droop gains. Therefore, $E\{\Pi_{loss}^P\}$ can be minimized by maximizing all k_{P_i} for given upper limits on these gains. Furthermore, since there is no dependence on network topology, node connectivity does not play a role in the optimal choice of k_{P_i}. On the other hand, the directional derivative in (34) *is* a function of the direction k_{P_l}. So, for given heterogeneous gains, the directional descent can be non-uniform. This point will be further investigated in Section IV.

We next establish an upper bound on $E\{\Pi_{loss}^Q\}$.

Corollary 2: If $E\{\mathrm{w}_0\mathrm{w}_0^T\}=I$,

$$E\{\Pi_{loss}^Q\} \;\le\; \frac{\alpha(2\bar{b}+\lambda_N)k_{Q_N}}{2\tau_Q\left(1+(2\bar{b}+\lambda_N)k_{Q_N}\right)}\sum_{i=1}^{N}k_{Q_i}^{-1}, \tag{29}$$

where $k_{Q_N}:=\max_i\{k_{Q_i}\}$.

Proof: See Appendix. ∎

The bound in (29) depends on the network topology only via the maximum eigenvalue of L_B instead of the eigenvalues and the eigenvectors of L_Q. It also asymptotically goes to zero in the limit of large reactive power gains. Although $E\{\Pi_{loss}^Q\}$ is not necessarily monotonically decreasing in the gains, for given k_{Q_N} this bound provides a worst case performance value that is decreasing in all $k_{Q_i}\neq k_{Q_N}$.

IV. Numerical Examples

We now numerically investigate the dependence of the transient resistive losses on the changes in heterogeneous droop gains for $E\{\mathrm{w}_0\mathrm{w}_0^T\}=I$. The parameter values are $\alpha=0.2$, $\bar{b}=\tau_Q=1$ in all simulations. The directional derivative (34) is plotted with respect to non-uniform active power gains $k_{P_i}\in\{1,\ldots,50\}$ in Figure 4 (left). It can be observed that the steepest descent in $E\{\Pi_{loss}^P\}$ occurs in the direction of the smallest gain. Furthermore, the degree of descent monotonically decreases as the magnitude of the perturbed gain increases. As a result, in this particular example the amount of performance improvement is inversely related to the magnitude of the perturbed gain. Therefore, heterogeneous active power sharing requirements (equivalently heterogeneous inverter ratings F_P) might limit performance, regardless of the network topology and line properties. Analytical exploration of this observation is a direction for future work.

In the case of a complete graph with unit edge weights, which dictates uniform topology dependence of all nodes, a similar behavior is observed from Figure 4 (right) for $\frac{\Delta E\{\Pi^Q_{loss}\}}{\Delta k_{Q_i}}$, i.e. the estimation of the directional derivative of $E\{\Pi^Q_{loss}\}$ with respect to $k_{Q_i} \in \{1,\dots,50\}$. We estimate this derivative by choosing a perturbation of $\Delta k_{Q_i} = 10^{-5}$. As before, performance improvement is inversely related to the magnitude of the perturbed gain.

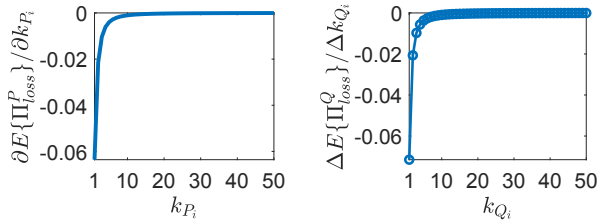

Fig. 4: Directional derivative of $E\{\Pi^P_{loss}\}$ with respect to k_{P_i} (left), and a numerical estimate of the directional derivative of $E\{\Pi^Q_{loss}\}$ with respect to k_{Q_i} for a complete graph of unit edge weights (right) with $E\{\mathrm{w}_0\mathrm{w}_0^T\} = I$.

We next investigate (for $E\{\mathrm{w}_0\mathrm{w}_0^T\} = I$) how line susceptances affect the rate of change in $E\{\Pi_{loss}\}$ due to a change in each node's droop gain. We only consider $E\{\Pi^Q_{loss}\}$ since $E\{\Pi^P_{loss}\}$ does not depend on the network topology. We consider a complete graph with edge weights drawn from the uniform distribution over the interval $(0, 1]$ and assign uniform gains via $F_Q = I$ and $k_Q = 1$. Using a perturbation of $\Delta k_{Q_i} = 10^{-5}$, $\frac{\Delta E\{\Pi^Q_{loss}\}}{\Delta k_{Q_i}}$ is plotted with respect to the perturbed node i in Figure 5. Here the nodes are sorted by increasing weighted degree. The general trend is that a larger performance improvement is observed for unit change in the droop gain as the weighted degree increases. However this relationship is not monotonic. In several instances this general trend is not seen, which can be explained as follows. $E\{\Pi^Q_{loss}\}$ depends on the eigenvalues and eigenvectors of the scaled Laplacian L_Q as well as the inverter ratings F_Q per Theorem 3. Since the weighted degrees are non-uniform, each gain perturbation leads to possibly non-uniform perturbations in the eigenvalues and the eigenvectors of L_Q. So, the perturbation terms in $E\{\Pi^Q_{loss}\}$ can result in a non-monotonic relationship with increasing weighted degree.

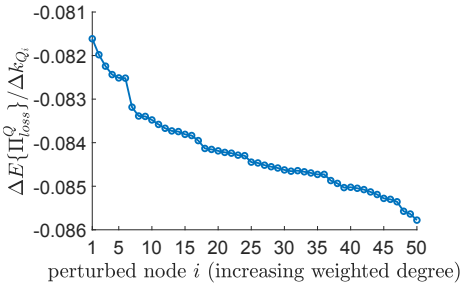

Fig. 5: A numerical estimate of the directional derivative of $E\{\Pi^Q_{loss}\}$ with respect to k_{Q_i} for a complete graph with edge weights drawn from the uniform distribution over $(0, 1]$, where $E\{\mathrm{w}_0\mathrm{w}_0^T\} = I$.

V. Conclusions and Directions for Future Work

This work generalized previous performance analysis concerning uniform nodal dynamics in droop-controlled microgrids to the case of heterogeneously rated inverters. Our result for the frequency and voltage synchronization performance emphasizes the possible problem of inertia in inverter-based systems. We also demonstrated that the transient resistive losses are sensitive to the heterogeneity in droop gains, hence power sharing requirements can limit performance. Extension to the case of coupled frequency-voltage dynamics is a direction for future work.

Appendix

Proof of Lemma 1

Equations (24) and (25) follow from (7), using (19) and (23) in the time-domain. A realization for (20) is given by

$$h_i^{P,\omega} = \left(\begin{array}{c|c} A_i & B_i \\ \hline C_i & 0 \end{array}\right),$$

where $A_i = \begin{bmatrix} 0 & 1 \\ -\frac{k_P}{\tau_P}\lambda_i^P & -\frac{1}{\tau_P} \end{bmatrix}$, $B_i = \begin{bmatrix} 0 \\ \frac{1}{\tau_P} \end{bmatrix}$, $C_i = \begin{bmatrix} 0 & 1 \end{bmatrix}$. The inner product in (24) can be computed by [18]

$$\langle h_i^{P,\omega},\, h_j^{P,\omega}\rangle \;=\; \int_0^\infty [h_i^{P,\omega}(t)]^T h_j^{P,\omega}(t)dt \;=\; B_i^T X_{ij} B_j,$$

where X_{ij} is the solution to the Sylvester equation

$$A_i^T X_{ij} + X_{ij} A_j = -C_i^T C_j. \tag{30}$$

The inner product $\langle h_i^Q,\, h_j^Q\rangle$ in (25) can be similarly computed using the following time-domain realization for (22)

$$h_i^Q = \left(\begin{array}{c|c} \frac{-1-k_Q\lambda_i^Q}{\tau_Q} & \frac{1}{\tau_Q} \\ \hline 1 & 0 \end{array}\right). \tag{31}$$

Proof of Lemma 2

We can rewrite (10) as

$$\Pi_{loss} = \alpha \int_0^\infty \Big[\theta(t)^T L_B \theta(t) \;+\; V(t)^T(2\bar{b}I + L_B)V(t)\Big]dt - 2\alpha\bar{b}\|V\|^2_{\mathcal{L}_2},$$

which by using (18) and (23) in the time-domain leads to

$$\Pi_{loss} = \alpha \int_0^\infty \Big[(z_0^P)^T \tilde{H}^P(t) R_\perp^T L_P R_\perp \tilde{H}^P(t) z_0^P \;+\; (z_0^Q)^T H^Q(t) U^T L_Q U H^Q(t) z_0^Q\Big]dt - 2\alpha\bar{b}\|V\|^2_{\mathcal{L}_2}. \tag{32}$$

Here $R_\perp^T L_P R_\perp = \mathrm{diag}\{\lambda_i^P\}_{i=2,\dots,N} =: \tilde{\Lambda}_P$ and we recall that $U^T L_Q U = \Lambda_Q$ which leads to

$$\int_0^\infty \tilde{H}^P(t)\tilde{\Lambda}_P\tilde{H}^P(t)dt \;=\; \mathrm{diag}\{\lambda_i^P\|h_i^P(t)\|^2_{\mathcal{L}_2}\}_{i=2,\dots,N},$$
$$\int_0^\infty H^Q(t)\Lambda_Q H^Q(t)dt \;=\; \mathrm{diag}\{\lambda_i^Q\|h_i^Q(t)\|^2_{\mathcal{L}_2}\}.$$

The realization of h_i^P in (17) is given by $h_i^P = \left(\begin{array}{c|c} A_i & B_i \\ \hline C_i & 0 \end{array}\right)$, where $A_i = \begin{bmatrix} 0 & 1 \\ -\frac{k_P}{\tau_P}\lambda_i^P & -\frac{1}{\tau_P} \end{bmatrix}$, $B_i = \begin{bmatrix} 0 \\ \frac{1}{\tau_P} \end{bmatrix}$, $C_i = \begin{bmatrix} 1 & 0 \end{bmatrix}$. Then $\|h_i^P(t)\|^2_{\mathcal{L}_2} = B_i^T X_{ii} B_i$ where X_{ii} solves (30) for $i = j$, which is a Lyapunov equation. Similarly the realization of h_i^Q in (31) leads to

$$\|h_i^P(t)\|^2_{\mathcal{L}_2} = \frac{1}{2k_P\lambda_i^P},\; \|h_i^Q(t)\|^2_{\mathcal{L}_2} = \frac{1}{2\tau_Q\left(1 + k_Q\lambda_i^Q\right)}. \tag{33}$$

Substituting these expressions and $\|V\|_{\mathcal{L}_2}^2 = (z_0^Q)^T \Psi_Q z_0^Q$ from Lemma 1 into (32) yields the first result. Taking the limit of Π_{loss} as $k_P \to \infty$ and $k_Q \to \infty$ and using $\Psi_Q \to 0$ from the proof of Theorem 2 leads to the second result.

Proof of Corollary 1

The partial derivative of $E\{\Pi_{loss}^P\}$ with respect to k_{P_l} is

$$\frac{\partial E\{\Pi_{loss}^P\}}{\partial k_{P_l}} = \frac{\alpha}{2k_{P_l}^2}\left(-1 + \frac{2k_{P_l}^{-1}}{\sum_{i=1}^N k_{P_i}^{-1}} - \frac{\sum_{i=1}^N k_{P_i}^{-2}}{\left(\sum_{i=1}^N k_{P_i}^{-1}\right)^2}\right) \quad (34)$$

$$= \alpha\left(\frac{-k_{P_l}\sum_{i=1}^N k_{P_i}^{-2} - k_{P_l}\sum_{j=1}^N\sum_{i=1}^{j-1}(k_{P_i}k_{P_j})^{-1} + \sum_{i=1}^N k_{P_i}^{-1}}{k_{P_l}^3\left(\sum_{i=1}^N k_{P_i}^{-1}\right)^2}\right),$$

where we used the fact that $\left(\sum_{i=1}^N k_{P_i}^{-1}\right)^2 = \sum_{i=1}^N k_{P_i}^{-2} + 2\sum_{j=1}^N\sum_{i=1}^{j-1}(k_{P_i}k_{P_j})^{-1}$. So $\frac{\partial E\{\Pi_{loss}^P\}}{\partial k_{P_l}} < 0$ if and only if

$$\kappa_l := -k_{P_l}\left(\sum_{i=1}^N k_{P_i}^{-2} + \sum_{j=1}^N\sum_{i=1}^{j-1}(k_{P_i}k_{P_j})^{-1}\right) + \sum_{i=1}^N k_{P_i}^{-1} < 0.$$

Partitioning the double summation over a triangular region,

$$\sum_{j=1}^N\sum_{i=1}^{j-1}(k_{P_i}k_{P_j})^{-1} = \sum_{i=1}^{l-1}(k_{P_i}k_{P_l})^{-1} + \sum_{j=l+1}^N (k_{P_l}k_{P_j})^{-1} + \Xi_l,$$

where $\Xi_l = \sum_{j=1}^{l-1}\sum_{i=1}^{j-1}(k_{P_i}k_{P_j})^{-1} + \sum_{j=l+1}^N\sum_{i=1}^{l-1}(k_{P_i}k_{P_j})^{-1} + \sum_{j=l+2}^N\sum_{i=l+1}^{j-1}(k_{P_i}k_{P_j})^{-1}$. Substituting this expression into κ_l gives $\kappa_l = -k_{P_l}\left(\sum_{i\in\{1,\dots,N\}\setminus l} k_{P_i}^{-2} + \Xi_l\right) < 0$, which completes the proof since $l \in \{1,\dots,N\}$ is arbitrary.

Proof of Corollary 2

Recalling that $\Sigma^Q = 2\alpha\bar{b}\|V\|_{\mathcal{L}_2}^2 \geq 0$, the following holds

$$E\{\Pi_{loss}^Q\} \leq \frac{\alpha}{2\tau_Q}\sum_{i=1}^N \frac{u_i^T F_Q^{-1} u_i}{k_Q + \frac{1}{\lambda_i^Q}}, \quad (35)$$

due to Theorem 3. Using the definition of L_Q given by (13) and (15), one can write for $i = 1,\dots,N$

$$\frac{\lambda_i^Q}{u_i^T F_Q u_i} = \frac{u_i^T F_Q^{\frac{1}{2}}(2\bar{b}I + L_B)F_Q^{\frac{1}{2}}u_i}{u_i^T F_Q u_i} \in \mathrm{conv}(\{2\bar{b} + \lambda_j\}),$$

where $\mathrm{conv}(\cdot)$ denotes the convex hull and we used the numerical range of the symmetric matrix $2\bar{b}I + L_B$ [21]. Then $\lambda_i^Q \in \mathrm{conv}\left(\{u_i^T F_Q u_i(2\bar{b} + \lambda_j)\}\right)$, which leads to

$$\lambda_i^Q \leq \max_j\{u_i^T F_Q u_i(2\bar{b} + \lambda_j)\} = u_i^T F_Q u_i(2\bar{b} + \lambda_N).$$

Finally noting that $\lambda_i^Q \leq \max_i\{\lambda_i^Q\} \leq (2\bar{b} + \lambda_N)\frac{k_{Q_N}}{k_Q}$, substituting into (35) and using $\sum_{i=1}^N u_i^T F_Q^{-1} u_i = \mathrm{tr}(U^T F_Q^{-1} U) = \mathrm{tr}(F_Q^{-1})$ yields the result.

REFERENCES

[1] M. C., Chandorkar, D. M., Divan, and R. Adapa, "Control of Parallel Connected Inverters in Standalone AC Supply Systems," IEEE Trans. on Industry Applications, vol. 29, no. 1, pp. 136 – 143, 1993.

[2] K. De Brabandere, B. Bolsens, J. Van den Keybus, A. Woyte, J. Driesen, and R. Belmans, "A Voltage and Frequency Droop Control Method for Parallel Inverters," IEEE Trans. on Power Electronics, vol. 22, no. 4, pp. 1107 – 1115, 2007.

[3] J. W. Simpson-Porco, F. Dörfler, and F. Bullo, "Synchronization and Power Sharing for Droop-controlled Inverters in Islanded Microgrids," Automatica, vol. 49, no. 9, pp. 2603 – 2611, 2013.

[4] B. Gentile, J. Simpson-Porco, F. Dörfler, S. Zampieri, and F. Bullo, "On Reactive Power Flow and Voltage Stability in Microgrids," in Proc. of the American Ctrl. Conf., June 2014, pp. 759 – 764.

[5] J. Schiffer, R. Ortega, A. Astolfi, J. Raisch, and T. Sezi, "Conditions for Stability of Droop-controlled Inverter-based Microgrids," Automatica, vol. 50, no. 10, pp. 2457 – 2469, 2014.

[6] J. Schiffer, T. Seel, J. Raisch, and T. Sezi, "Voltage Stability and Reactive Power Sharing in Inverter-based Microgrids with Consensus-based Distributed Voltage Control," IEEE Trans. on Ctrl. Systems Technology, vol. 24, no. 1, pp. 96 – 109, 2016.

[7] P. Vorobev, P. H. Huang, M. Al Hosani, J. L. Kirtley, and K. Turitsyn, "A Framework for Development of Universal Rules for Microgrids Stability and Control," in Proc. of the 56^{th} IEEE Conf. on Dec. and Ctrl., Dec. 2017, pp. 5125 – 5130.

[8] E. Tegling, B. Bamieh, and D. Gayme, "The Price of Synchrony: Evaluating the Resistive Losses in Synchronizing Power Networks," IEEE Trans. on Ctrl. of Network Systems, vol. 2, no. 3, pp. 254 – 266, 2015.

[9] E. Sjödin and D. Gayme, "Transient Losses in Synchronizing Renewable Energy Integrated Power Networks," in Proc. of the American Ctrl. Conf., June 2014, pp. 5217 – 5223.

[10] E. Tegling, D. F. Gayme, and H. Sandberg, "Performance Metrics for Droop-controlled Microgrids with Variable Voltage Dynamics," in Proc. of the 54^{th} IEEE Conf. on Dec. and Ctrl., Dec. 2015, pp. 7502 – 7509.

[11] T. W. Grunberg and D. F. Gayme, "Performance Measures for Linear Oscillator Networks over Arbitrary Graphs," IEEE Trans. on Ctrl. of Network Systems, vol. 5, no. 1, pp. 456 – 468, Mar. 2018.

[12] H. G. Oral, E. Mallada, and D. F. Gayme, "Performance of First and Second Order Linear Networked Systems Over Digraphs," in Proc. of the 56^{th} IEEE Conf. on Dec. and Ctrl., Dec. 2017, pp. 1688 – 1694.

[13] M. Pirani, J. W. Simpson-Porco, and B. Fidan, "System-Theoretic Performance Metrics for Low-Inertia Stability of Power Networks," in Proc. of the 56^{th} IEEE Conf. on Dec. and Ctrl., Dec. 2017, pp. 5106 – 5111.

[14] T. W. Grunberg and D. F. Gayme, "Minimizing Interactions in Mixed Oscillator Networks," in Proc. of the 53^{rd} IEEE Conf. on Dec. and Ctrl., Dec. 2014, pp. 3209 – 3215.

[15] B. K. Poolla, S. Bolognani, and F. Dörfler, "Optimal Placement of Virtual Inertia in Power Grids," IEEE Trans. on Automatic Ctrl., vol. 62, no. 12, pp. 6209 – 6220, Dec. 2017.

[16] E. Tegling, M. Andreasson, J. Simpson-Porco, H. Sandberg, "Improving Performance of Droop-Controlled Microgrids Through Distributed PI-Control," in Proc. of the American Ctrl. Conf., Jul. 2016, pp. 2321 – 2327.

[17] Y. Jiang, R. Pates, and E. Mallada, "Performance Tradeoffs of Dynamically Controlled Grid-connected Inverters in Low Inertia Power Systems," in Proc. of the 56^{th} IEEE Conf. on Dec. and Ctrl., Dec. 2017, pp. 5098 – 5105.

[18] F. Paganini and E. Mallada, "Global Performance Metrics for Synchronization of Heterogeneously Rated Power Systems: The Role of Machine Models and Inertia," in Proc. of the 55^{th} Allerton Conf. on Communication, Ctrl., and Computing, Oct. 2017, pp. 324 – 331.

[19] L. Guo, C. Zhao, and S. H. Low, "Graph Laplacian Spectrum and Primary Frequency Regulation," in Proc. of the 57^{th} IEEE Conf. on Dec. and Ctrl., Dec. 2018, pp. 158 – 165.

[20] F. Dörfler and F. Bullo, "Kron Reduction of Graphs with Applications to Electrical Networks," IEEE Trans. on Circuits and Systems I, vol. 60, no. 1, pp. 150 – 163, Jan 2013.

[21] R. A. Horn and C. R. Johnson, "Matrix Analysis," Cambridge University Press, 2012.

[22] A. E. Motter, S. A. Myers, M. Anghel, and T. Nishikawa, "Spontaneous Synchrony in Power-grid Networks," Nature Physics, vol. 9, no. 3, pp. 191 – 197, Feb. 2013.